Three-dimensional analysis of the surface mode supported in Čerenkov and Smith-Purcell free-electron lasers

Yashvir Kalkal* and Vinit Kumar†

Homi Bhabha National Institute, Mumbai 400094, India

Accelerator and Beam Physics Laboratory, Raja Ramanna Centre for Advanced Technology, Indore 452013, India

(Received 7 August 2015; published 10 June 2016)

In Čerenkov and Smith-Purcell free-electron lasers (FELs), a resonant interaction between the electron beam and the copropagating surface mode can produce a copious amount of coherent terahertz radiation. We perform a three-dimensional (3D) analysis of the surface mode, taking the effect of attenuation into account, and set up 3D Maxwell-Lorentz equations for both these systems. Based on this analysis, we determine the requirements on the electron beam parameters, i.e., beam emittance, beam size and beam current for the successful operation of a Čerenkov FEL.

DOI: 10.1103/PhysRevAccelBeams.19.060702

I. INTRODUCTION

The Čerenkov free-electron laser (CFEL) [1–18] and the Smith-Purcell free-electron laser (SP-FEL) [19–31], which use low-energy electron beam [9–18,21–31] are seen as compact, and tunable sources of coherent terahertz (THz) radiation. This radiation can be utilized for a variety of applications in material science, biophysics and industrial imaging [32,33].

In a CFEL, an electron beam skims over the surface of a thin dielectric slab placed over an ideal conductor and resonantly interacts with the copropagating electromagnetic surface mode supported by the system, resulting in emission of coherent radiation. The SP-FEL is similar to the CFEL, except that the "dielectric slab placed over an ideal conductor" is replaced with a metallic reflection grating. Over the past few decades, several efforts have been made to realize the generation of coherent radiation from CFEL [4–9,12–14] and SP-FEL [21,29,30] systems. The coherent emission of radiation with average power of the order of tens of μW was reported from a single slab based CFEL at ENEA Frascati Centre [5,8]. Subsequently, Fisch and Walsh [9] used a low energy electron beam (∼30–200 keV) to drive a sapphire based CFEL. An efficient and compact version of the device described in Ref. [9], which uses a very low energy (∼30 keV) electron beam, was tested at the Dartmouth College [12] for the generation of THz radiation. The observed output power in the Dartmouth experiment [12] was very low (∼ picowatt), and authors in Ref. [12] suggested that a good quality flat electron beam can be used to enhance the output power of the system. Recently, under the joint research of Osaka Sangyo University and Kansai University, experimental studies on a double slab based CFEL have been performed [13,14]. Experimental studies on the SP-FEL system have been performed at Dartmouth College [21] and Vanderbilt University [29] in the USA, and CEA/Cesta [30] in France. The power level attained in all these experiments have been low. In order to obtain a copious coherent radiation from the Čerenkov and Smith-Purcell FELs, an enhanced understanding of these systems is required, which includes analyzing the realistic effects due to diffraction and attenuation of the surface mode supported by these systems, and then working out the requirement on electron beam parameters, which is very critical for the performance of the system. Although for the case of the SP-FEL, the requirements on electron beam parameters taking the effect of diffraction and attenuation [24] have been worked out in Refs. [26–28], a similar analysis has not been presented for the case of the CFEL. In this paper, we perform such an analysis to work out the electron beam requirements for the case of the CFEL, taking the effect due to diffraction and attenuation into account. While doing so, we also highlight important differences in the analyses of the CFEL and the SP-FEL.

A schematic of Čerenkov FEL is shown in Fig. 1, where a flat electron beam is skimming at a height h over a thin dielectric slab placed over an ideal conductor. The surface mode supported in this system is evanescent in the x-direction. Most of the earlier analyses [3,10,11,17,18] of the CFEL have been performed under two-dimensional (2D) approximation, where the surface mode is assumed to have translational invariance along the y-direction, and it is therefore nonlocalized. In Ref. [18], we have performed a rigorous 2D analysis of CFELs by setting up the Maxwell-Lorentz

*yashvirkalkal@gmail.com
†vinit@rrcat.gov.in

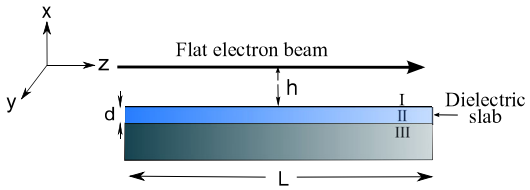

FIG. 1. Schematic of Čerenkov FEL driven by a flat electron beam.

equations in both the linear and the nonlinear regime. It was shown that for the generation of THz radiation in a CFEL, the required beam profile is thin in the vertical direction, and wide in the horizontal direction. Hence, we used a flat electron beam with vanishing thickness in the vertical direction and infinite width in the horizontal direction, in our analysis. The analytical expressions for the small-signal gain and growth rate of the CFEL were derived for this case. In a realistic situation, the electron beam size as well as the radiation beam size will be finite. Size of the radiation beam will increase due to diffraction. This will affect the overlap of the radiation beam with the electron beam, resulting in reduction of the small-signal gain, as well as the saturated power obtained in the device. A realistic estimate of diffraction effects therefore requires a detailed three-dimensional (3D) analysis of the electromagnetic surface mode.

One way to invoke 3D effects is to solve the electromagnetic Helmholtz wave equation by considering the diffraction in the surface mode. Andrew and Brau [15] assumed the electron beam as a plasma dielectric and solved the wave equation with diffraction effects to evaluate the growth rate of the CFEL. This approach works well in the linear regime. Growth rate was found to be decreasing on the accounts of the 3D effects as compared to the 2D analysis. In Ref. [15], the analysis was performed for an uniform electron beam having infinite vertical size, hence, the derived results are not very useful to obtain the electron beam parameters in the vertical direction.

Another way to consider the 3D effects, which we follow in this paper, is to construct a localized surface mode by combining the plane waves propagating at different angles in the (y, z) plane, with a suitable weight factor. The surface mode constructed in this way is localized in the horizontal direction and represents a realistic situation. The technique of localization of electromagnetic modes by using superposition of plane waves is a standard technique in laser optics discussions also [34–36], and has been applied for the case of grating based FEL by Kim and Kumar [26–28].

Our paper is organized as follows. In Sec. II A, we review the 2D analysis of Čerenkov FEL [18], and then perform the analysis for the 3D localized surface modes in Sec. II B. In Sec. II C, we set up the 3D coupled Maxwell-Lorentz equations for the CFEL system. Earlier analyses of CFEL in single slab geometry have neglected the effect of attenuation due to dielectric and conductor, which we include in the analysis presented in Sec. II. Next, in Sec. III A, we review the 2D analysis of the Smith-Purcell FEL [25,26]. We then set up the 3D coupled Maxwell-Lorentz equations for the SP-FEL system in Sec. III B and highlight the differences compared to the case of CFEL. Considering the effect of diffraction, the requirements on the quality of electron beam for the successful operation of such devices become very stringent, which is discussed in Sec. IV A for the case of the Čerenkov FEL. We also discuss the techniques to relax these stringent requirements, and also the methods for production of electron beam of required quality. In Sec. IV B, we take a specific example to show that with achievable beam quality, it should be possible to generate a copious amount of terahertz radiation in a Čerenkov FEL, even after including the three-dimensional effects and effects due to attenuation. Finally, we discuss the results, and present some conclusions in Sec. V.

II. SURFACE MODE ANALYSIS IN A ČERENKOV FEL

In this section, we first review the 2D analysis of beam-wave interaction in a CFEL, where we have added the effect of attenuation due to finite conductivity of the metallic conductor and also the dielectric losses, which was not present in the earlier analysis [18]. Details of calculation of the attenuation coefficient are given in the Appendix. Next, we set up a localized surface mode and discuss its important properties in Sec. II B. Finally, in Sec. II C, we present the derivation of the three-dimensional equation for the evolution of the surface mode.

A. Review of two-dimensional analysis

The geometry of a Čerenkov FEL with the coordinate system used in our analysis is shown in Fig. 1. An electron beam with vanishing thickness in the x-direction is propagating with a velocity v along the z-direction at a height h above the dielectric surface. The dielectric slab has length L, thickness d and relative dielectric constant ϵ. The dielectric slab extends uniformly along the y-axis, and the 2D electromagnetic surface mode supported by this structure does not have any variation along the y-direction. To have an effective interaction with the electron beam, we want the electric field component in the z-direction. The appropriate surface mode for this structure can be taken as the TM mode, which has the magnetic field only in the y-direction, namely H_y and the components of the electric field can be obtained from H_y by using the Maxwell equation. The longitudinal component of the electric field is given by

$$E_z(x, z, t) = Ee^{i\psi}e^{-\Gamma x}, \tag{1}$$

where E is the amplitude of the field at the location of the electron beam i.e., $x = 0$, $\psi = k_0 z - \omega t$ is the electron phase, k_0 is the propagation wave number in the

z-direction, $\omega = 2\pi c/\lambda$, c is the speed of light, λ is the free-space wavelength and $\Gamma = \sqrt{k_0^2 - \omega^2/c^2}$ is a positive quantity, which means that the amplitude of the surface mode decays in the x-direction.

The electron beam interacts with the copropagating surface mode and develops microbunching at the wavelength of the surface mode. This results in a sinusoidal component of electron beam current, having frequency ω and wave number k_0, the same as that of the surface mode. This component of the beam current generates an evanescent electromagnetic wave, again having frequency ω and wave number k_0, and an amplitude that decays exponentially with distance from the beam. The evanescent wave is incident on the dielectric surface and gets reflected with a reflectivity $R = i\chi/\nu + \chi_1$, where χ and χ_1 are constants, which depend on ω, k_0, and intrinsic parameters of the system. Here, ν is the growth rate of the incident evanescent wave, which is physically understood as resulting due to exponential enhancement in the microbunching, as the beam propagates, due to its interaction with the surface mode. An analytical formula for the reflectivity is derived by satisfying the appropriate boundary conditions at different interfaces in Fig. 1, and this gives the expressions for χ and χ_1, which are provided in Ref. [18]. Note that in this approach, if $\nu = 0$, the reflectivity becomes singular, for frequency ω and wave number k_0 satisfying the dispersion relation. In that case, the dielectric slab placed on the metallic conductor supports the surface electromagnetic mode in the absence of any incident wave, as expected. The reflected wave further interacts with the copropagating electron beam, resulting in enhancement of microbunching, and consequently the amplitude of the incident evanescent wave further increases. This phenomenon continues until the amplitude of the surface mode saturates due to nonlinearity. The evolution of the amplitude E of the surface mode discussed here is mathematically described by the following time-dependent differential equation, which includes attenuation of the surface mode:

$$\frac{\partial E}{\partial z} + \frac{1}{\beta_g c}\frac{\partial E}{\partial t} = \frac{-Z_0\chi}{2\beta\gamma}\frac{dI}{dy}e^{-2\Gamma h}\langle e^{-i\psi}\rangle - \alpha E, \tag{2}$$

where $\beta_g = v_g/c$ is the group velocity of the surface mode in unit of c, which can be computed from the dispersion curve of the surface mode. The dispersion relation is here given by $\sqrt{\epsilon\omega^2/c^2 - k_0^2}\tan(d\sqrt{\epsilon\omega^2/c^2 - k_0^2}) = \epsilon\sqrt{k_0^2 - \omega^2/c^2}$, which is obtained requiring the condition that the reflectivity R becomes singular. The first term on the right-hand side of Eq. (2) represents the interaction of the electron beam with the surface mode, where $Z_0 = 1/\epsilon_0 c = 377\ \Omega$ is the characteristic impedance of free space, ϵ_0 is the permittivity of free space, $\beta = v/c$, γ is the relativistic Lorentz factor, I represents the electron beam current, dI/dy is the linear current density of flat electron beam and $\langle\cdots\rangle$ indicates averaging over the number of particles distributed over one wavelength of the evanescent surface mode. The second term on the right-hand side of Eq. (2) represents attenuation of the surface wave due to losses present in the dielectric and metallic structures. Note that the above equation without the attenuation term is described in Ref. [18]. The attenuation coefficient α is the sum of the dielectric attenuation coefficient α^d and Ohmic attenuation coefficient α^c due to losses present in the metallic conductor. As derived in detail in the Appendix, the attenuation coefficient of the surface mode in a CFEL is given by

$$\alpha = \frac{\gamma k_0 Z_0 \tan\delta(2 - \epsilon\beta^2) + \beta\epsilon^2 k_0(1 + a^2)(2R_s + \beta k_0 Z_0 d\tan\delta)}{2Z_0[\gamma(1 + \epsilon^2 a^2) + \epsilon k_0 d(1 + a^2)]}. \tag{3}$$

Here, $\tan\delta$ represents tangent loss of the dielectric medium, $a = (\gamma/\epsilon)\sqrt{\epsilon\beta^2 - 1}$, $R_s = \sqrt{\mu_0\omega/2\Sigma}$ is surface resistance of the metal, μ_0 is the permeability of free space and Σ represents conductivity of the metal. We would like to mention that the effect of attenuation on the performance of the single slab CFEL system has been ignored in all the previous analyses. In this paper, we will show that to obtain a meaningful gain in a CFEL system, one has to minimize the losses due to attenuation in the surface mode.

In a CFEL based on a positive refractive index dielectric, the surface mode will have a positive group velocity v_g and will be amplified as it propagates with the electron beam in the positive z-direction [15]. When the amplified field is fed back at the entrance of the interaction region by using an optical cavity, the system starts working as an oscillator. The electron trajectories will evolve due to interaction with the electromagnetic field of the surface mode. Here, the electron motion is assumed to be strictly in the longitudinal direction, and the equations for the evolution of energy and phase of the ith electron are given by [18]

$$\frac{\partial\gamma_i}{\partial z} + \frac{1}{\beta c}\frac{\partial\gamma_i}{\partial t} = \frac{eE}{m_0 c^2}e^{i\psi_i} + \text{c.c.}, \tag{4}$$

$$\frac{\partial\psi_i}{\partial z} + \frac{1}{\beta c}\frac{\partial\psi_i}{\partial t} = \frac{\omega}{c\beta^3\gamma^2}\left(\frac{\gamma_i - \gamma_p}{\gamma_p}\right). \tag{5}$$

Here, e is the electronic charge, m_0 is the mass of electron, and the subscript p is meant for the resonant particle, whose velocity is equal to the phase velocity of the surface mode. The behavior of a Čerenkov FEL is governed by the Maxwell equation given by Eq. (2) together with

Lorentz equations given by Eqs. (4) and (5). The set of Eqs. (2), (4), and (5) can be solved numerically to obtain the detailed behavior of the CFEL system in both the linear and the nonlinear regime, as described in Ref. [18]. In the small-signal small-gain regime, an analytical solution of Eqs. (2), (4), and (5) has been obtained for the small-signal gain as [18]

$$G = 4 \times 6.75 \times 10^{-2} \times 2\pi \frac{\chi}{I_A} \frac{k_0 L^3}{\beta^3 \gamma^4} \frac{dI}{dy} e^{-2\Gamma h}, \quad (6)$$

where $I_A = 4\pi\epsilon_0 m_0 c^3/e = 17.04$ kA is the Alfvén current. The factor $e^{-2\Gamma h}$ is a measure of the interaction between the electron beam and the copropagating evanescent surface mode. Taking the effect of attenuation, there will be a round-trip loss given by $(1 - e^{-4\alpha L})$ in addition to the gain described by Eq. (6). In the small-signal high-gain regime, growth rate of a CFEL using monoenergetic flat electron beam is given by [18]

$$\nu = \frac{\sqrt{3}}{2L} \left(2\pi \frac{\chi}{I_A} \frac{k_0 L^3}{\beta^3 \gamma^4} \frac{dI}{dy} e^{-2\Gamma h} \right)^{1/3}. \quad (7)$$

Taking the effect of attenuation, the growth rate will reduce to $\nu - \alpha$.

B. Localized surface mode

Now, we consider the effect of diffraction of the surface mode in the y-direction and construct the 3D localized surface mode supported in a CFEL system. As the dielectric slab is an open structure in the y-direction, the supported electromagnetic surface mode is expected to behave like a freely propagating optical beam and will undergo diffraction in the (y, z) plane. The diffracting electromagnetic surface mode can be constructed by combining the plane waves propagating at different angles in the (y, z) plane, with suitable weight function $A(k_y)$ in k_y as

$$E_z(x, y, z, t) = \frac{1}{\sqrt{2\pi}} \int dk_y A(k_y) e^{i(k_z z - \omega t)} e^{ik_y y} e^{-\Gamma' x}. \quad (8)$$

Here, E_z is the longitudinal electric field, Γ' is the attenuation constant due to evanescent nature in the x-direction, when the wave is propagating in the (y, z) plane with wave numbers k_y and k_z in the y-direction and the z-direction respectively. The surface mode constructed in this way will have a variation along the y-direction and will represent the generalized case of surface mode given by Eq. (1). The electromagnetic surface mode given by Eq. (8) is mainly propagating in the z-direction and undergoes diffraction in the y-direction.

In the CFEL system, the dielectric slab is an isotropic structure in the (y, z) plane. Using the property of isotropy in the (y, z) plane, the dispersion relation of the surface mode propagating along the z-axis can be easily generalized to the case, where the surface mode is propagating along any arbitrary direction in the (y, z) plane. For a given frequency ω, if the phase velocity of the surface mode propagating along the z-axis is v, we obtain the following relation between ω, k_y and k_z for a surface wave propagating in the (y, z) plane:

$$\omega = v\sqrt{k_y^2 + k_z^2}. \quad (9)$$

The wave number in the longitudinal direction can be written as $k_z = k_0 + \Delta k$, where $k_0 = \omega/v$. By using the paraxial approximation ($k_y \ll k_z$), we obtained the following expression for k_z:

$$k_z = k_0 \left(1 - \frac{k_y^2}{2k_0^2} \right). \quad (10)$$

Note that due to the property of isotropy in the (y, z) plane, $\Gamma' = \Gamma$. We can substitute Eq. (10) for k_z and $\Gamma' = \Gamma$ in Eq. (8) to obtain the localized surface mode in a CFEL as

$$E_z(x, y, z, t) = \frac{e^{i\psi} e^{-\Gamma x}}{\sqrt{2\pi}} \int \underbrace{A(k_y) e^{-ik_y^2 z/2k_0}} e^{ik_y y} dk_y. \quad (11)$$

The above expression for the longitudinal field appears as a Fourier transform in k_y of the underbraced term. If we choose $A(k_y) = e^{-k_y^2/2\sigma_{k_y}^2}$, the integration in Eq. (11) is a Fourier transform of a Gaussian function. Gaussian functions belong to the distinct family of functions which are self-Fourier functions [37]. Hence, the resultant of integration in Eq. (11) is also a Gaussian function, and we obtain the intensity for the localized Gaussian mode at $x = 0$ as

$$\text{Intensity}: E_z \times E_z^* \propto e^{-\frac{y^2}{2} \frac{2\sigma_{k_y}^2}{1 + \sigma_{k_y}^4 z^2/k_0^2}}. \quad (12)$$

We want to emphasize that this approach can be easily generalized for higher order modes by taking Gauss-Hermite functions for $A(k_y)$, which are also self-Fourier functions and will give higher order Gauss-Hermite modes.

Next, we analyze the transverse properties of the localized surface mode. Using Eq. (12), we obtain an expression for the variation of rms optical beam size σ_y with z as

$$\sigma_y^2(z) = \sigma_y^2(0) \left(1 + \frac{z^2}{Z_R^2} \right). \quad (13)$$

Here, $\sigma_y(0)$ is the rms optical beam waist at $z = 0$ and Z_R is the Rayleigh range which is obtained as

$$Z_R = \frac{4\pi\sigma_y^2(0)}{\beta\lambda}. \tag{14}$$

Another quantity of interest is the product of rms beam waist size and rms angular divergence σ_θ, which is given as

$$\sigma_y(0) \times \sigma_\theta = \frac{\beta\lambda}{4\pi}. \tag{15}$$

Note that the above expressions are similar to the standard expressions for the case of a Gaussian mode propagating in free space except that λ is replaced with $\beta\lambda$. It is well known in optics that for a Gaussian mode propagating in a uniform, isotropic medium, λ gets replaced with λ/n in the above formulas, where n is the refractive index of the medium. Using $n = c/v_p$, where v_p is phase velocity of light in the medium, λ/n is the same as $(v_p/c)\lambda$. This is thus similar to the result we obtained for the surface mode here.

The present analysis for the localized surface mode will be used to estimate the required parameters of the electron beam for efficient working of the Čerenkov FEL in Sec. IV.

C. Three-dimensional Maxwell-Lorentz equations

Next, we will derive the three-dimensional Maxwell-Lorentz equations for the CFEL system. We start with the generalized expression for the sinusoidal component of the beam current density: $\mathcal{J} = J(x,y)e^{i(k_0 z-\omega t)}\langle e^{-i\psi}\rangle + \text{c.c.}$, where $J(x,y)$ is the dc current density, $\langle e^{-i\psi}\rangle$ indicates bunching of the electron beam due to interaction with the surface mode and c.c. represents complex conjugate. We can decompose the beam current density into Fourier components as

$$\mathcal{J} = \frac{1}{\sqrt{2\pi}}\int \underbrace{\tilde{J}(x,k_y)e^{ik_y^2 z/2k_0}\langle e^{-i\psi}\rangle}_{} e^{i\psi} e^{-ik_y^2 z/2k_0} e^{ik_y y} dk_y + \text{c.c.} \tag{16}$$

Note that we have cast the integral in a form such that the Fourier component of the electromagnetic field can be understood to be evolving with the Fourier component of the electron beam current density. For further calculations, we consider the flat electron beam for which $J(x,y) = j(y)\delta(x)$ and its Fourier transform is written as $\tilde{J}(x,k_y) = \tilde{j}(k_y)\delta(x)$. The electromagnetic fields due to this current density can be obtained by using Maxwell equations under appropriate boundary conditions, and we obtain the longitudinal component of electric field as

$$E_z(x,y,z,t) = \frac{e^{i\psi}e^{-\Gamma x}}{\sqrt{2\pi}}\int \underbrace{A(k_y,z,t)}_{} e^{-ik_y^2 z/2k_0} e^{ik_y y} dk_y + \text{c.c.} \tag{17}$$

The amplitude $A(k_y,z,t)$ of the surface mode will evolve due to interaction with the copropagating electron beam and we have assumed it to be a slowly varying function of z and t. The beam-wave interaction in a CFEL system for the 2D case is discussed earlier in Sec. II A. Now, by following the same approach and realizing that the underbraced term in Eq. (17), which is the amplitude of Fourier component of the electromagnetic field, is evolving due to interaction with the amplitude of corresponding Fourier component of the current density, denoted by the underbraced terms in Eq. (16), we obtain the following time dependent differential equation for the evolution of $A(k_y,z,t)$:

$$\frac{\partial A}{\partial z} + \frac{1}{\beta_g c}\frac{\partial A}{\partial t} = \frac{-Z_0\chi}{2\beta\gamma}\tilde{j}(k_y)e^{ik_y^2 z/2k_0}e^{-2\Gamma h}\langle e^{-i\psi}\rangle - \alpha A. \tag{18}$$

By taking the Fourier transform with respect to k_y in Eq. (18) and using the fact that $Ae^{-ik_y^2 z/2k_0}$ is the Fourier transform of the longitudinal surface field, we obtain the following differential equation for the 3D surface mode:

$$\frac{\partial E}{\partial z} - \frac{i}{2k_0}\frac{\partial^2 E}{\partial y^2} + \frac{1}{\beta_g c}\frac{\partial E}{\partial t} = \frac{-Z_0\chi}{2\beta\gamma}\frac{dI}{dy}e^{-2\Gamma h}\langle e^{-i\psi}\rangle - \alpha E. \tag{19}$$

Here, E is the amplitude of longitudinal field E_z and dI/dy is the linear current density of the flat beam. The second term on the left-hand side of the above equation represents diffraction of the surface mode and allows us to study the transverse profile of the optical beam. In an approximate way, the effect of partial overlap between the electron beam and optical mode can be considered in the numerical solutions of 2D Maxwell-Lorentz equations by writing the linear current density dI/dy as $I/\Delta y$, where Δy is the electron beam width, and is replaced with the effective optical beam width determined using Eq. (14).

III. SURFACE MODE ANALYSIS IN A SMITH-PURCELL FEL

The essential features of the analysis of surface mode supported in a SP-FEL system have been worked out earlier in Refs. [25–28]. Here, we further elaborate to highlight the interesting difference in the analyses of CFEL and SP-FEL systems. We first review the 2D analysis, which is followed by the 3D analysis of the surface mode, where we provide derivations of some important results and present a comparison with the case of CFELs.

A. Review of two-dimensional analysis

As shown in Fig. 2, a metallic reflection grating is used as the slow wave structure in an SP-FEL. Here, the supported surface mode is a combination of Floquet space harmonics, since the grating is a periodic structure. The zeroth-order component will show the strongest interaction with the electron beam and has a similar structure as given

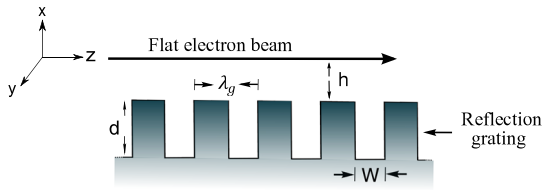

FIG. 2. Schematic of a Smith-Purcell FEL, using a flat electron beam.

by Eq. (1) [25]. Similar to the case of the CFEL described in the previous section, the electron beam interacts with the copropagating surface mode and the dynamical equation for the evolution of the amplitude of surface mode is given by [25,26]

$$\frac{\partial E}{\partial z}-\frac{1}{\beta_g c}\frac{\partial E}{\partial t}=\frac{Z_0\chi}{2\beta\gamma}\frac{dI}{dy}e^{-2\Gamma h}\langle e^{-i\psi}\rangle+\alpha E. \tag{20}$$

Here, the calculation of χ requires numerical evaluation of R as a function of growth rate for a given value of (ω, k_0) of the surface mode, and details regarding the procedure for this calculation are described in Ref. [25]. Evaluation of the attenuation coefficient α requires calculation of heat dissipation at metallic surfaces for the given surface mode, which has been discussed for the case of the SP-FEL in Ref. [24]. Note the difference in sign of terms containing β_g, χ and α in the above equation as compared to Eq. (2) for the CFEL. This is due to the fact that the SP-FEL has negative group velocity for the surface mode, as described in Ref. [25], whereas the group velocity is positive in case of the CFEL system. The negative group velocity for the SP-FEL makes it a backward-wave oscillator (BWO) and oscillations build up when the linear current density dI/dy exceeds a threshold value dI_s/dy [25,26]:

$$\frac{dI}{dy}>\frac{dI_s}{dy}=\mathcal{J}(\eta)\frac{I_A\beta^4\gamma^4}{2\pi\chi kL^3}e^{2\Gamma h}. \tag{21}$$

Here, $\mathcal{J}(\eta)$ represents dimensionless start current as a function of the loss parameter $\eta=\alpha L$ and $k=\omega/c$, and is evaluated in Ref. [38].

After having briefly discussed the 2D analysis, we next discuss the localized surface mode and set up the 3D coupled Maxwell-Lorentz equations for the SP-FEL system.

B. Localized surface mode and three-dimensional Maxwell-Lorentz equations

In order to construct the localized surface mode, we need to combine the plane waves propagating at different angles in the (y, z) plane with suitable weight function. In order to perform this calculation, we need to know the 3D dispersion relation, i.e., the dependence of ω on k_z, for different values of k_y. As discussed in Sec. II A, the dispersion relation is obtained by deriving the condition for singularity in R. In an SP-FEL system, the calculation of R of the grating for growing evanescent waves for the 2D case was carried out by Kumar and Kim [39] and the dispersion relation of the surface mode was obtained. This analysis was then extended by including the $\exp(ik_y y)$-type variation in the electromagnetic (em) field and reflectivity was evaluated [28] for the 3D case. A remarkable observation in their analysis is that if we replace ω by $\sqrt{\omega^2-c^2k_y^2}$ in the expression for the reflectivity for the case $k_y=0$, we obtain the reflectivity for the 3D case, where a finite value of k_y is considered [28,31]. This is because here we have electromagnetic field present only in one medium, i.e., the space above the surface of the reflection grating (including the grooves of the grating), which is in vacuum. Due to this feature, the expression for reflectivity has terms like $(\omega^2-c^2k_z^2)$ in the 2D case, which can be simply replaced with $(\omega^2-c^2k_y^2-c^2k_z^2)$ for the 3D case. This amounts to replacing ω in the 2D case by $\sqrt{\omega^2-c^2k_y^2}$, to determine the dispersion relation for the 3D case with finite k_y.

It is important here to note the difference between the dispersion relation of the SP-FEL and the CFEL system. A careful observation of the 2D dispersion relation of the CFEL, $\sqrt{\epsilon\omega^2/c^2-k_0^2}\tan(d\sqrt{\epsilon\omega^2/c^2-k_0^2})=\epsilon\sqrt{k_0^2-\omega^2/c^2}$ [18], indicates that the simple "replacement rule" as in the case of the SP-FEL system, i.e., replacing ω in 2D dispersion relation with $\sqrt{\omega^2-c^2k_y^2}$, will not give us the 3D dispersion relation. This is because here, the electromagnetic field in CFEL is present in vacuum as well as in the dielectric medium, unlike the SP-FEL case; therefore terms like $(\omega^2-c^2k_o^2)$ as well as $(\omega^2-c^2k_o^2/\epsilon)$ appear in the 2D dispersion relation. In the case of the CFEL, the "isotropic nature" of the dielectric slab in the (y, z) plane facilitates us to analyze the diffraction in the surface mode as described in the previous section. The grating structure used in the SP-FEL system has grooves along the surface in the transverse direction and lacks isotropic behavior in the (y, z) plane. Due to this difference, the optical properties of the surface mode in the SP-FEL system are different as compared to the CFEL system, as elaborated below.

We now discuss the construction of the localized surface mode in the SP-FEL. Due to the replacement rule, $\omega_{3D}(k_y)=\sqrt{\omega_{2D}^2+(ck_y)^2}$, we write the longitudinal wave number k_z as

$$k_z=k_0+\left.\frac{\partial k}{\partial\omega}\right|_{k_y=0}\Delta\omega, \tag{22}$$

where $\Delta\omega=\omega_{2D}-\omega_{3D}$ and the term $\partial k/\partial\omega$ at $k_y=0$ is identified as $(-1/\beta_g c)$. Using these results along with the paraxial approximation in Eq. (22), we obtain

$$k_z = k_0\left(1+\frac{k_y^2}{2\beta\beta_g k_0^2}\right). \tag{23}$$

Here, we note the difference between the above equation and the corresponding equation [Eq. (10)] for the case of the CFEL. On account of 3D effects, the magnitude of change in the longitudinal wave number ($|k_z - k_0|$) is given by $\beta\lambda k_y^2/4\pi$ for the CFEL and $\lambda k_y^2/4\pi\beta_g$ for the SP-FEL case. It can be seen that in this term, $\beta\lambda$ in the case of the CFEL is replaced with λ/β_g for the case of the SP-FEL.

Next, by satisfying the wave equation for the electromagnetic field, we obtain the expression for Γ' as

$$\Gamma' = \Gamma\left(1+\frac{k_y^2(1+\beta\beta_g)}{2\beta\beta_g\Gamma^2}\right). \tag{24}$$

By following an approach similar to the one described in Sec. II B, the analysis for the localized surface mode supported by the grating structure is performed. The Rayleigh range for the optical surface mode is obtained as [26]

$$Z_R = \frac{4\pi\beta_g\sigma_y^2(0)}{\lambda}, \tag{25}$$

where $\sigma_y(0)$ is the rms beam size at the waist. Under paraxial approximation, the product of rms beam waist size and rms divergence is given by [26]

$$\sigma_y(0)\times\sigma_\theta = \frac{\lambda}{4\pi\beta_g}. \tag{26}$$

Note that Eqs. (25) and (26) have dependence on the group velocity, while equivalent quantities in the CFEL system [Eqs. (14) and (15)] have dependence on the phase velocity of the surface mode. In these expressions, the term $\beta\lambda$ in the case of the CFEL is replaced with λ/β_g in the case of the SP-FEL, as expected. We emphasize that this difference arises due to a fundamental difference in the way the dispersion relation for the two systems gets modified for the 3D case, which we have explained. Due to this nature, it can be seen that the diffraction effects are more prominent in the case of the SP-FEL as compared to the CFEL. The length L of the grating in the case of the SP-FEL has to be kept small to maintain sufficient interaction of the surface mode with the copropagating electron beam.

Next, the expression for k_z and Γ' can be used in Eq. (8) to set up the three-dimensional electromagnetic surface mode for the SP-FEL. By following the procedure described in Sec. II C, the following time dependent three-dimensional differential equation for the evolution of the surface mode in a SP-FEL is obtained [28]:

$$\frac{\partial E}{\partial z}+\frac{i}{2\beta\beta_g k_0}\frac{\partial^2 E}{\partial y^2}-\frac{1}{\beta_g c}\frac{\partial E}{\partial t}=\frac{Z_0\chi}{2\beta\gamma}\frac{dI}{dy}e^{-2\Gamma h}\langle e^{-i\psi}\rangle+\alpha E. \tag{27}$$

Note the difference in the second term of the above equation as compared to the corresponding term in Eq. (19) for the CFEL. Here, a factor $\beta\beta_g$ is appearing, which shows large diffraction in the surface mode in an SP-FEL, as compared to the CFEL. Note that although the diffraction term in the above equation has the same form as in the case of the undulator based FEL [40], the free-space wavelength λ appearing in this term for the undulator based FEL is replaced with $\beta\lambda$ in the CFEL and λ/β_g in the SP-FEL, and this is an important finding of our analysis. We would like to mention here that although Ref. [28] describes Eq. (27), it does not elaborate on the procedure to derive this equation, which is provided in this paper.

IV. ELECTRON BEAM REQUIREMENTS AND ITS PRODUCTION FOR THE ČERENKOV FEL

In this section, based of the analysis of the surface mode presented in Sec. II B, we will work out the electron beam requirements for successful operation of a CFEL. Similar analysis for the SP-FEL has already been worked out in Refs. [26,27], which we extend to the case of the CFEL in this section.

A. Theoretical analysis

The electron beam distribution in the four-dimensional phase space (x, ψ, y, ϕ) is assumed to be Kapchinskij-Vladimirskij (KV) distribution [41], where x and y are the vertical and horizontal coordinates respectively, and ψ and ϕ represent vertical and horizontal angles, respectively. The electron beam distribution is assumed to have half-widths (Δx, $\Delta\psi$, Δy, $\Delta\phi$) at the middle of the dielectric slab and the half-widths are 2 times the rms values (σ_x, σ_ψ, σ_y, σ_ϕ). Thus, $\Delta x = 2\sigma_x$, $\Delta\psi = 2\sigma_\psi$, $\Delta y = 2\sigma_y$ and $\Delta\phi = 2\sigma_\phi$. The geometric rms emittance in the y-direction is therefore given by $\boldsymbol{\varepsilon}_y^0 = (1/4)\Delta y\Delta\phi$. The Courant-Snyder envelope β_y, also known as the beta function in the y-direction, is defined as $\beta_y = \sigma_y^2/\boldsymbol{\varepsilon}_y^0$. Similar quantities are defined with the subscript x in the x-direction.

Let us first look for the requirements on the electron beam in the y-direction. The product of rms beam size $\sigma_y(o)$ and divergence σ_θ for the surface mode supported in the CFEL is given by $\beta\lambda/4\pi$. Now to ensure that electron beam envelope is within the envelope of optical beam, the rms unnormalized emittance is required to be less than this product. Applying this for the case of the CFEL, we get

$$\boldsymbol{\varepsilon}_y \le \frac{\beta^2\gamma\lambda}{4\pi}, \tag{28}$$

where $\boldsymbol{\varepsilon}_y = \beta\gamma\boldsymbol{\varepsilon}_y^0$ is the normalized beam emittance in the y-direction. Next, the half-width Δy of the electron beam,

which is taken the same as the half-width $2\sigma_y$ of the optical beam, is chosen by requiring that the Rayleigh range Z_R is equal to the interaction length L. This choice of Z_R ensures that the variation in the rms optical beam size over the interaction length is within 10%, as can be seen by putting $z = L/2$ ($z = 0$ corresponds to middle of the dielectric slab and $z = \pm L/2$ corresponds to the end points), and $Z_R = L$ in Eq. (13). Now, by using Eq. (14), we find $\sigma_y = \sqrt{\beta\lambda Z_R/4\pi}$ and by inserting it in the above-mentioned condition, we obtain

$$\Delta y = \sqrt{\frac{\beta\lambda L}{\pi}}. \tag{29}$$

Let us now discuss the required electron beam parameters in the x-direction. In the view of the exponential factor $e^{-2\Gamma h}$ in Eq. (6), it is desirable that the height h of the electrons should satisfy $h \leq 1/2\Gamma$ for the sufficient interaction between the electron beam and the copropagating surface mode. Here, $\Gamma = 2\pi/\beta\gamma\lambda$. Assuming that the electron beam is propagating over the dielectric slab such that its centroid is at height h and its lower edge just touches the dielectric surface, we can take the half-width Δx of the electron beam the same as $h = 1/2\Gamma$, and obtain

$$\Delta x = \frac{\beta\gamma\lambda}{4\pi}. \tag{30}$$

This implies that rms electron beam size $\sigma_x = \Delta x/2 = \beta\gamma\lambda/8\pi$ at the middle of the dielectric slab. In order to ensure that the variation in σ_x over the interaction length is less than $\sim$10%, we require $\beta_x \geq L$. Using these two conditions and the relation that $\boldsymbol{\varepsilon}_x^0 = \sigma_x^2/\beta_x$, we obtain

$$\boldsymbol{\varepsilon}_x \leq \frac{\beta^3\gamma^3\lambda^2}{64\pi^2 L}, \tag{31}$$

where $\boldsymbol{\varepsilon}_x = \beta\gamma\boldsymbol{\varepsilon}_x^0$ is the normalized beam emittance in the x-direction. The condition on the normalized beam emittance $\boldsymbol{\varepsilon}_x$ comes out to be very stringent. As discussed in detail in the next subsection, a flat electron beam with transverse emittance ratio, $\boldsymbol{\varepsilon}_y/\boldsymbol{\varepsilon}_x \simeq 1000$ is required for the operation of a practical CFEL. This value is roughly 10 times higher than the value achieved in a recent experiment [42].

The stringent requirement on the emittance of a flat electron beam can be relaxed by introducing an external focusing by either using a wiggler field [43,44] or by using a solenoid field [45,46]. Details of the two schemes are described in Ref. [27] for the case of the SP-FEL. Both schemes are applicable for the case of the CFEL also. We briefly discuss these schemes for the CFEL case and give the relevant mathematical formulas here.

1. Focusing of flat beam by using a wiggler field

In the first scheme, where a wiggler magnetic field is used for external focusing, the flat electron beam is generated by a novel phase space technique [26,47]. In this technique, a cathode is placed in an axial magnetic field to produce a round beam and then the angular momentum of beam is removed by using a set of quadrupoles. Finally, a flat electron beam is obtained with transverse emittance ratio [26]:

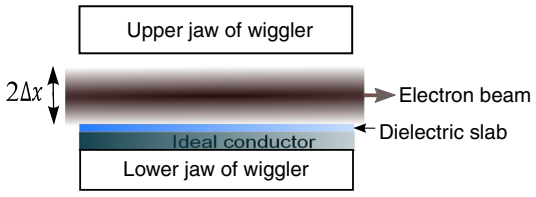

FIG. 3. Schematic of external focusing in a Čerenkov FEL using a wiggler.

$$\frac{\boldsymbol{\varepsilon}_y}{\boldsymbol{\varepsilon}_x} = \left(\frac{eB}{m_0 c}\frac{r_t^2}{4\boldsymbol{\varepsilon}_I}\right)^2, \tag{32}$$

where B represents the magnetic field at the cathode, r_t is the radius of the thermionic cathode, and $\boldsymbol{\varepsilon}_I = \sqrt{\boldsymbol{\varepsilon}_x\boldsymbol{\varepsilon}_y}$ is the initial beam emittance of the round beam. The radius r_t is related to the initial emittance as $r_t = 2\boldsymbol{\varepsilon}_I/\sqrt{k_B T/m_0 c^2}$ [26], where k_B is Boltzmann's constant and T is the absolute temperature of the thermionic cathode. The magnetic field required to produce an electron beam with the desired transverse emittance ratio is evaluated by using Eq. (32) as $B = k_B T/e\boldsymbol{\varepsilon}_x c$. Note that B is independent of $\boldsymbol{\varepsilon}_y$. The current density J_t at the cathode for a given beam current I is $J_t = I/\pi r_t^2$ [26].

In Fig. 3, we have shown the schematic for focusing of the above-mentioned flat beam in a CFEL by using a wiggler with a parabolic pole shape. In the presence of a wiggler magnetic field, the electron beam will be focused in both x- and y-directions. By neglecting the space charge effect in the envelope equation, the matched rms beam size in the x- and y-directions is obtained as [27]

$$\sigma_{x,y} = 2^{1/4}\sqrt{\frac{\boldsymbol{\varepsilon}_{x,y}}{a_u k_{x,y}}}. \tag{33}$$

Here, $a_u = eB_u/k_u m_0 c$, B_u represents the peak value of the magnetic field in the x-direction, along the z-axis, $k_u = 2\pi/\lambda_u$, λ_u is the wiggler period, and k_x and k_y represent spatial frequency of the wiggler field in the x- and the y-direction, respectively. We require $k_u^2 = k_x^2 + k_y^2$ to satisfy the Maxwell equations. In Eq. (33), we choose $\sigma_y = 1/2\Delta y$ and $\sigma_x = 1/2\Delta x$, where Δy and Δx are given by Eqs. (29) and (30) respectively, and find the appropriate value of a_u, k_x and k_y for a given values of emittances ($\boldsymbol{\varepsilon}_x$, $\boldsymbol{\varepsilon}_y$), such that the beam sizes are matched inside a wiggler and thus maintain a constant size throughout the wiggler. For a typical set of parameters of a CFEL, the

focusing requirement in the vertical direction is very strong as compared to the horizontal direction; we can therefore choose $k_y = 0$ and $k_x = k_u$. It is clear from Eq. (33) that for a matched beam size, one can tolerate relaxed vertical emittance by choosing the higher value of the peak undulator magnetic field B_u. Note that in the case of external focusing in the vertical direction, we do not require to satisfy Eq. (31).

2. Focusing of flat beam by using solenoid field

In the second scheme, a solenoid magnetic field is used to focus a low energy flat electron beam. The required flat beam is generated using an elliptically shaped, planar thermionic cathode with major axis $\Delta y_c = \Delta y$ and minor axis $\Delta x_c = \Delta x$. The normalized thermal emittances for the thermionic cathode are given by $(\boldsymbol{\varepsilon}_x, \boldsymbol{\varepsilon}_y) = 0.5(\Delta x_c, \Delta y_c)\sqrt{k_B T/m_0 c^2}$, and current density at the cathode, corresponding to current I is given by $J_c = I/\pi \Delta x_c \Delta y_c$ [26]. For generating a flat beam, the vertical dimension of the cathode is very small compared to the horizontal dimension, and such a cathode is called a line cathode. The dielectric slab together with the line cathode is placed inside the solenoid and, in order to ensure that the beam does not rotate, the electron beam is generated in the uniform field region of the solenoid, and it remains inside the solenoid while propagating over the surface of the dielectric slab. The solenoid field strength required to focus a flat beam can be evaluated with the condition that the Larmor radius should be much smaller than the vertical rms beam size σ_x [27], which gives us the following expression for the axial magnetic field $B(0)$ near the cathode [27]:

$$B(0) \gg \frac{m_0 c \boldsymbol{\varepsilon}_x}{e\sigma_x^2}. \tag{34}$$

The nonuniformity in the longitudinal on-axis magnetic field gives rise to rotation θ to the flat beam given by [27]

$$\theta(z) = \frac{z\omega_L}{3\beta c}\frac{\Delta B(z)}{B(0)}, \tag{35}$$

where $\Delta B(z) = B(z) - B(0)$ and ω_L is the Larmor frequency. Here, it is assumed that the cathode is placed at the center of the solenoid ($z = 0$), where the field is maximum, and the variation of the quantities in the radial direction is assumed to be very slow. We have to ensure that the electron beam does not rotate significantly such that the flat beam nature is preserved. Also, there could be problems with the transmission of a flat beam by using a uniform solenoid magnetic field at higher beam currents as discussed earlier in Refs. [48,49], where it is pointed out that due to $E_s \times B(0)$ drift, where E_s is the electric field from space charge, the flat beam gets vertical kick in the opposite direction at its two edges, which results in the edge curling phenomenon. Beyond a certain threshold, this leads to an instability known as diocotron, and/or filamentation instabilities [48], which can disrupt the flat nature of the electron beam, resulting in significant interception of the beam. An analytic estimate for the threshold length L_D, after which the diocotron instability grows exponentially, can be given by $L_D\ (\mathrm{cm}) \simeq 800\beta^2\gamma^3 B(0)\ (\mathrm{kG})/J_c\ (\mathrm{A/cm^2})$ [48]. It can be seen that for a given beam energy and focusing field strength, the diocotron instability is suppressed at low beam current densities J_c or equivalently at reduced effective space charge, which is actually the case for the parameters considered in our analysis as discussed in detail in the next subsection.

Clearly, both external focusing techniques allow us to tolerate larger emittance of the electron beam, but these also increase the deleterious effects of the velocity spread. Due to external focusing, the spread in the longitudinal velocity is given by [27]

$$\frac{\Delta\beta}{\beta} \sim \frac{\boldsymbol{\varepsilon}_x^2}{2\beta^2\gamma^2\sigma_x^2}. \tag{36}$$

Focusing in the y-direction will also give a similar contribution to the velocity spread. Spread in the longitudinal velocity is equivalent to the spread in the energy. The maximum energy spread that can be tolerated in a CFEL corresponds to the phase mismatch of π between the electrons and the copropagating surface mode at the exit of the interaction region, or equivalently $\Delta\beta L/\beta = \beta\lambda/2$. This condition gives us the maximum value of emittance which can be tolerated by the system as

$$\boldsymbol{\varepsilon}_x < \sigma_x\sqrt{\frac{\beta^3\gamma^2\lambda}{L}}. \tag{37}$$

With the external focusing, we can increase the length L of the dielectric slab to obtain the maximum gain. However, the increment in L will restrict the maximum emittance that can be tolerated, a condition given in Eq. (37). We need to choose an optimum length of the system for which the deleterious effect due to resulting energy spread is significantly less.

Finally, we summarize the procedure for the optimization of the focusing strength and the emittance as follows: We first choose the vertical beam size from Eq. (30) for the given parameters of a CFEL, and then we choose the maximum focusing strength by using Eq. (33) (in the case of wiggler focusing) or using Eq. (34) (in the case of solenoid focusing) to attain the maximum tolerance on the vertical emittance, keeping in mind that the constraint is given by Eq. (37).

B. An example case

For an example case of a practical CFEL, we take parameters of the Dartmouth experiment [12], and optimize them in accordance with the analysis given in the earlier sections. In the Dartmouth experiment [12], an electron

beam with 1 mA current and with energy range 30–40 keV was allowed to pass over the dielectric slab of thickness 350 μm. Two different materials, GaAs ($\epsilon = 13.1$) and sapphire ($\epsilon = 9.6$), were used for the dielectric slab, and a silver polished copper metal was used to support the dielectric slabs. We choose sapphire as the dielectric material, which has very low tangent loss ($\tan\delta \leq 10^{-4}$) as compared to GaAs ($\tan\delta \simeq 10^{-3}$) [50]. We take the electron beam energy as 46.5 keV, corresponding to $\beta = 0.4$ ($\beta\gamma = 0.44$), which is well above the threshold condition ($\beta_t = 1/\sqrt{\epsilon} = 0.32$) for the generation of Čerenkov radiation in sapphire. For these parameters, we find $\lambda = 2.7$ mm, $\beta_g = 0.27$ and $\chi = 317$ per m by using the analysis given in Ref. [18]. The conductivity of silver metal at 300 K is given by $6.3 \times 10^7/\Omega$-m [51], for which the attenuation coefficient, $\alpha = 2.2$ per m, as calculated by using Eq. (3). Note that the dielectric losses in sapphire are negligible for the chosen parameters. In the context of 3D analysis, the linear current density dI/dy, which is needed to evaluate the gain and the growth rate of the system by using Eqs. (6) and (7) respectively, can be interpreted as the peak value at the middle of the electron beam distribution, which is given by [26]

$$\frac{dI}{dy} = \frac{I}{\pi\Delta y/2}, \tag{38}$$

for KV distribution discussed in Sec. IV A. The effective electron beam width in the y-direction is thus taken as π times the rms optical beam waist size $\sigma_y(0)$ and can be evaluated by using Eq. (29). The electron beam height, h is taken as half beam width Δx in the x-direction. The length of the dielectric slab was taken as 1 cm in the Dartmouth experiment. For $L = 1$ cm, we find a small signal gain of around 0.03%, which is too low to overcome losses present in the system, as the round-trip loss ($1 - e^{-4\alpha L}$) is around 8.4%. To get an appreciable gain, we take $L = 5$ cm and increase the electron beam current from 1 mA to 35 mA. By using the modified parameters in Eqs. (6) and (7), we find gain as 50% and growth rate as 21.2 per m respectively. With the increased length, power loss due to attenuation also increases. To reduce the attenuation, we propose that the silver metal, which supports the dielectric slab, should be kept at very low temperature i.e., at 77 K, which is the boiling point temperature of liquid nitrogen. The conductivity of silver at 77 K is about $3.3 \times 10^8/\Omega$-m [51], which gives us $\alpha = 0.97$ per m and round-trip loss of 17.6% over an interaction length of 5 cm. In order to attain saturation, the system is operated in the oscillator configuration, where a set of mirrors is used to provide an external feedback. One mirror is assumed to be ideal with 100% reflectivity of the field amplitude and other has reflectivity of 98%. The Maxwell-Lorentz equations have been solved numerically by using the leapfrog scheme [18] to obtain the power in the surface mode. The power builds up slowly and saturates after 100 number of passes, as shown by the solid curve in Fig 4. At saturation, we obtain the output power as 7.2 W. The input electron beam power is 1.6 kW, which gives us efficiency of 0.44%. Figure 4 also shows the output power (dashed curve) of a CFEL, where Ohmic losses are assumed to be zero. In this case, the CFEL system gives 41.3 W output power on saturation, with an efficiency of 2.5%. Note that the presence of Ohmic losses on the metallic surface severely affects the output power and efficiency of a CFEL system, and one has to optimize the system for minimum losses.

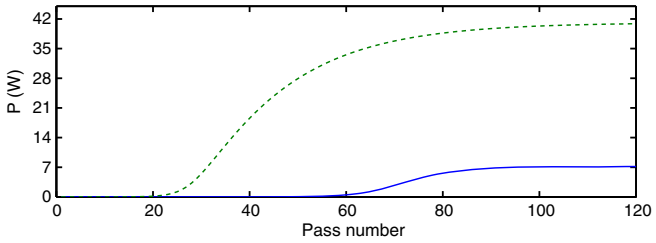

FIG. 4. Plot of output power as a function of pass number for the optimized parameters of a Čerenkov FEL discussed in the text. The dashed curve represents the case, where Ohmic losses are assumed to be zero, and the solid curve shows the output power with finite Ohmic losses in the system at 77 K temperature. The linear current density (dI/dy) of the electron beam is taken as 5.4 A/m.

The requirements on electron beam sizes are evaluated by using Eqs. (29) and (30), as $\Delta y = 4.2$ mm in the y-direction and $\Delta x = 94$ μm in the x-direction respectively. By using Eq. (31), we find that an electron beam with normalized vertical emittance $\boldsymbol{\varepsilon}_x \leq 1.9 \times 10^{-8}$ m-rad is needed in the absence of any external focusing, which is a very stringent requirement. In the horizontal direction, the condition on beam emittance is quite relaxed as an electron beam with $\boldsymbol{\varepsilon}_y \leq 3.8 \times 10^{-5}$ m-rad is required, which is calculated from Eq. (28). If we take $\boldsymbol{\varepsilon}_y = 1.9 \times 10^{-5}$ m-rad, which is 2 times less than the maximum allowed value, then a flat electron beam with transverse emittance ratio $\boldsymbol{\varepsilon}_y/\boldsymbol{\varepsilon}_x = 1000$ is required for the operation of the CFEL. In the Dartmouth experiment [12], these conditions have been clearly violated, where a round electron beam having large vertical emittance was used to drive the Čerenkov FEL. As discussed in the previous subsection, the transverse emittance ratio of 100 has been achieved experimentally [42] and it is feasible to extend this ratio to 400 [52].

To relax the stringent requirement on the electron beam emittance, external focusing can be provided by using a wiggler field as described in Sec. IV A 1. Here, we will take an explicit example to perform the calculations for the analytical results discussed in Sec. IV A 1. We assume a round electron beam with initial normalized emittance $\boldsymbol{\varepsilon}_I = 1 \times 10^{-6}$ m-rad, which is easily achievable. The flat electron beam can be produced by using round to flat beam transformation as discussed earlier and under this

transformation $\boldsymbol{\varepsilon}_I = \sqrt{\boldsymbol{\varepsilon}_x \boldsymbol{\varepsilon}_y}$. We choose the ratio of horizontal and vertical emittances as 100:1, i.e., $\boldsymbol{\varepsilon}_y = 10^{-5}$ m-rad and $\boldsymbol{\varepsilon}_x = 10^{-7}$ m-rad. This scheme requires an axial magnetic field $B = 37.4$ Gauss at the position of the cathode at $T = 1300$ K, which can be generated by using either a permanent magnet or an electromagnet [26]. The current density at the cathode, which is required to produce an electron beam of desired emittances discussed above, is obtained by using the prescription given in Sec. IV A 1 as $J_T = 0.06$ A/cm^2 at $T = 1300$ K. This value of current density can be easily achieved in thermionic cathodes e.g., oxide, dispenser and M-type cathodes [53,54], which can be operated for tens of thousands of hours at around 1300 K. Next, we discuss the requirements of the wiggler parameters to focus the flat beam described above. For a matched beam size $\sigma_x = 47$ μm and vertical emittance $\boldsymbol{\varepsilon}_x = 10^{-7}$ m-rad, we require $B_u = 1.1$ kG. This value of magnetic field can be obtained by using an array of regular pure permanent magnets in Halbach configuration, which gives a peak field strength of $1.7 B_{\rm rem} \exp(-\pi g/\lambda_u)$ [55], where $B_{\rm rem}$ is the remnant field of the magnetic material and g is the gap between the jaws of the wiggler. We have considered NdFeB as the magnetic material for which $B_{\rm rem} = 1.2$ T [55]. We have taken two cases for the wiggler gap, i.e., $g = 1$ mm and $g = 2$ mm, such that the beam transport is feasible. For $g = 1$ mm, we need a miniwiggler with 1.1 mm period and for $g = 2$ mm, we need a wiggler period of 2.2 mm, to obtain the required magnetic field of 1.1 kG. This type of mm or sub mm period wiggler can be fabricated by using the laser micromachining of bulk permanent magnets as discussed in Ref. [56]. We have checked that for the proposed wiggler field and wiggler period, the condition for the Mathieu stability of the wiggler focusing, i.e., $(e\lambda_u B_u/2\sqrt{2}\pi m_0 c\beta\gamma)^2 < 0.5$ [57], is satisfied. It has also been checked that the criteria for the maximum tolerance on beam emittance as given by Eq. (37) is easily met for the above discussed case.

Next, we discuss another possibility to relax the stringent requirement on the vertical beam emittance, where we can use a line cathode immersed in the solenoid field to produce a flat electron beam. This method has been discussed in detail in Sec. IV A 2. To produce a flat electron beam with beam half-widths $\Delta x = 94$ μm and $\Delta y = 4.2$ mm, we need a line cathode with $\Delta x_c = 94$ μm, and $\Delta y_c = 4.2$ mm. At $T = 1300$ K, we obtain $\boldsymbol{\varepsilon}_x = 2.2 \times 10^{-8}$ m-rad and $\boldsymbol{\varepsilon}_y = 9.7 \times 10^{-7}$ m-rad, which are quite acceptable. For beam current of 35 mA, the current density at the line cathode is obtained as $J_c = 2.86$ A/cm^2. Again, these cathode loadings (current density up to 10 A/cm^2) are trivial for the modern thermionic cathodes [53,54,58]. By using Eq. (34), we find that the solenoid magnetic field $B(0)$ is required to be greater than 0.17 kG to focus such a flat electron beam. We choose $B(0) = 1.0$ kG. The Larmor radius is obtained as 7.3 μm for these parameters, which is significantly smaller than the rms beam size $\sigma_x = 47$ μm. To keep the flat beam rotation less than 10 mrad over a length $L = 5$ cm, we require the field uniformity $\Delta B/B$ to be better than 0.4%, as calculated by using Eq. (35). We would like to mention that the considered electron beam is not space charge dominated as the space charge term is small compared to the emittance term in the envelope equation [41], i.e., $I\Delta x^3/4\beta\gamma I_A \boldsymbol{\varepsilon}_x^2(\Delta x + \Delta y) < 1$ for the x-direction. We have evaluated the left-hand side in this inequality and obtain 0.62. The condition in the y-direction is less restrictive for our case. For the beam current density of 2.86 A/cm^2 and axial magnetic field of 1.0 kG, we find the lower bound estimate for the diocotron instability growth length L_D as 58.0 cm. The proposed length of the CFEL system (5 cm) is about 12 times less than the threshold growth length, hence, the diocotron instability due to $E_s \times B(0)$ effect is not of concern in our system.

V. DISCUSSIONS AND CONCLUSIONS

In this paper, we have presented a three-dimensional analysis of the surface mode in Čerenkov FELs. Expressions have been derived for the electromagnetic field in a localized surface mode by suitably combining the plane wave solutions of Maxwell equations, propagating at different angles. A crucial input for this calculation was to have the information about the change in k_z, after we include $e^{ik_y y}$-type dependence in the electromagnetic field, keeping the value of ω fixed. For the case of the CFEL, this was simplified due to the "isotropic nature" of the system in the (y, z) plane, and in the case of the SP-FEL, this was simplified due to the "replacement rule" for the evaluation of reflectivity of the incident evanescent wave. Interestingly, the isotropic nature is not applicable for the SP-FEL case and the replacement rule is not applicable for the CFEL case.

Three-dimensional analysis of the surface mode allows us to include the effect of diffraction, which plays an important role in the performance of a CFEL. We have explained in the paper that for an isotropic system, as in the case of the CFEL, in the diffraction term in the wave equation, λ gets replaced with $\beta\lambda$. On the other hand if the system is not isotropic, but the em field is present only in vacuum, as in the case of the SP-FEL, λ gets replaced with λ/β_g. Diffraction results in partial overlapping between the electron beam and the copropagating optical mode. Consequently, the gain and the growth rate of a CFEL system reduce. To incorporate the 3D effects in the formulas for the gain and the growth rate calculations, we have taken the electron beam size to be the same as the effective optical beam size, which has been evaluated by taking the 3D variations in the surface mode.

We also derived expressions for dielectric losses and losses due to finite conductivity of the metal, which play an important role when we increase the interaction length in order to increase the gain in a CFEL. Although all earlier

analyses on the single slab CFEL have ignored this effect, it is important to take such realistic effects into account in a practical device, as is the case in any device using guided waves at high frequency. It is interesting to point out that even in the case of SP-FELs, the effect of attenuation was neglected in earlier studies, and its importance was realized in later studies [24,38]. In order to reduce the loss due to finite conductivity of metal in a CFEL, we have proposed that the metallic base can be kept at low temperature. We have optimized the parameters for a CFEL designed to operate at 0.1 THz and shown that using a 46.5 keV electron beam with a current of 35 mA, an optimized CFEL oscillator can deliver output power of 7.2 W at saturation with an efficiency of 0.44%.

Our overall approach is built on the earlier analyses given in Refs. [26,27], where the diffraction properties of the surface mode have been studied to determine the requirements on electron beam parameters for the successful operation of an SP-FEL. Here, our aim has been to perform the analysis for the CFEL case and find out the electron beam parameters for a practical CFEL system. Like the SP-FEL [27], the requirements on the vertical beam emittance in a CFEL come out to be stringent and we have discussed two ways to relax the stringent requirements. In the first scheme, a wiggler magnetic field is used to focus a flat electron beam, which is produced by a novel phase-space technique discussed in Ref. [26]. This scheme requires a peak wiggler field of about 1.1 kG to focus a flat electron beam having transverse emittance ratio $\boldsymbol{\varepsilon}_y/\boldsymbol{\varepsilon}_x = 100$. This value of transverse emittance ratio has been achieved recently at Fermi National Accelerator Laboratory [42] and well below the recently proposed value of 400 [52]. In the second scheme, we used a solenoid field to focus the flat electron beam, which is produced by a line shaped tungsten cathode placed at the center of the solenoid. The solenoid field is taken as 1 kG with field uniformity $\Delta B/B$ required to be better than 0.4% over a length of 5 cm. Although the suggested schemes may add to the complexity of the system, these are implementable and are needed to satisfy the stringent requirements for optimum performance of the system.

It is important to mention here that for the thermionic cathode, we have taken only the thermal emittance into consideration. In reality, the beam emittance could be larger than this [59]. We have checked that with suitable change in the parameters, our schemes would still work. For the case of wiggler focusing, this would require us to choose a smaller cathode size and hence, the beam current density at cathode would increase and also the magnetic field required at cathode for the flat beam production would increase. We have checked that even if the total emittance is twice the thermal emittance, the required current density and magnetic field required at cathode are increased by 4 times, and these values are still easily achievable. For the case of solenoid focussing, if we take the total emittance as twice the thermal emittance, the required minimum solenoid focusing field $B(0)$ increases by a factor of 2 and therefore becomes 0.34 kG. In our calculation, we have considered a solenoid focusing field of 1 kG, which is still higher than 0.34 kG.

We would like to mention that our analysis can be extended to understand the implications of 3D effects on working of a CFEL based on the other schemes such as using double slab [14,16] and negative refractive index material [17]. In the negative index material, the group velocity of the surface mode is negative. Due to the negative group velocity of the surface mode, the CFEL system works like a BWO [17]. The Čerenkov FEL in the BWO configuration can be studied by following an approach given in Refs. [25–27], where the working of Smith-Purcell FELs in BWO configuration is discussed.

To summarize, we have performed 3D analysis of the surface mode and set up 3D Maxwell-Lorentz equations for a CFEL and a SP-FEL system. We notice that the diffraction term appearing in Eqs. (19) and (27) is similar to the corresponding term for the case of the undulator based FEL [40,60]. Hence, the numerical techniques that are applied for the solution of such equations in typical 3D FEL codes such as GENESIS [61] can be extended for 3D simulation of CFEL and SP-FEL, which may be taken up in the future. The realistic effects such as the effect due to energy spread, and finite beam emittance can also be included in the computer code. We have optimized the parameters of a Čerenkov FEL by including the 3D effects, and attenuation due to dielectric and Ohmic losses, and find that the device can produce copious THz radiation, even after including these effects. Our analysis can be used for the detailed optimization of both the CFEL and the SP-FEL system.

ACKNOWLEDGMENTS

We thank anonymous referees for several helpful comments and suggestions. We acknowledge Professor S. B. Roy and Professor P. D. Gupta for their support and encouragement. One of us (Y. K.) gratefully acknowledges Homi Bhabha National Institute, Department of Atomic Energy (India) for the financial support.

APPENDIX: CALCULATIONS FOR THE ATTENUATION COEFFICIENT OF THE ELECTROMAGNETIC SURFACE MODE IN A ČERENKOV FEL

In this Appendix, we calculate the attenuation coefficient of the electromagnetic surface mode due to loss inside the dielectric slab and loss due to finite conductivity of the metal, which supports the dielectric slab. The schematic of the device is shown in Fig. 1, where free space is assigned as region I, dielectric slab as region II and the metallic base as region III. The electromagnetic fields in region I are

obtained by solving Maxwell equations with appropriate boundary conditions as [18]

$$H_y^I(x,z,t) = H\exp[i\psi - \Gamma(x+h)] + \text{c.c.}, \quad \text{(A1)}$$

$$E_x^I(x,z,t) = (HZ_0/\beta)\exp[i\psi - \Gamma(x+h)] + \text{c.c.}, \quad \text{(A2)}$$

$$E_z^I(x,z,t) = (-iHZ_0/\beta\gamma)\exp[i\psi - \Gamma(x+h)] + \text{c.c.} \quad \text{(A3)}$$

Here, H represents the magnetic field strength at the dielectric surface at $x = -h$. Electromagnetic fields in region II are given by [18]

$$H_y^{II}(x,z,t) = \frac{\epsilon\Gamma}{k_1}\frac{\cos[k_1(x+h+d)]}{\sin(k_1 d)}H\exp(i\psi) + \text{c.c.}, \quad \text{(A4)}$$

$$E_x^{II}(x,z,t) = \frac{k_0\Gamma}{\omega\epsilon_0 k_1}\frac{\cos[k_1(x+h+d)]}{\sin(k_1 d)}H\exp(i\psi) + \text{c.c.}, \quad \text{(A5)}$$

$$E_z^{II}(x,z,t) = \frac{-i\Gamma}{\omega\epsilon_0}\frac{\sin[k_1(x+h+d)]}{\sin(k_1 d)}H\exp(i\psi) + \text{c.c.}, \quad \text{(A6)}$$

where $k_1 = \sqrt{\epsilon\omega^2/c^2 - k_0^2}$. Total power transmitted by the electromagnetic fields is the sum of power flow in region I and region II, which can be obtained by integrating the Poynting vector over the area transverse to the direction of beam propagation. The expression for total transmitted power is obtained as [18]

$$\frac{P_t}{\Delta y} = \frac{Z_0 H^2}{\beta k_0 \epsilon^2 a^2}[\gamma(1+\epsilon^2 a^2) + \epsilon k_0 d(1+a^2)]. \quad \text{(A7)}$$

The attenuation coefficient of the surface wave is given by [62]

$$\alpha^{d,c} = \frac{P_l^{d,c}}{2P_t}, \quad \text{(A8)}$$

where, P_l is power loss per unit length along the z-direction, and the superscripts d and c are meant for the dielectric and metallic conductor respectively. In region II, namely the dielectric medium, losses are described with a complex relative permittivity $\tilde{\epsilon} = \epsilon - i\epsilon'$, where $\tan\delta = \epsilon'/\epsilon$ is identified as tangent loss of the dielectric medium [63]. Power loss per unit length in the dielectric medium can be written as $P_l^d = \epsilon_0\epsilon\omega\tan\delta\int(|E_x^{II}|^2 + |E_z^{II}|^2)dxdy$, where the integration is carried out from $-(h+d)$ to $-h$ in the x-direction and over length Δy in the y-direction. By using Eqs. (A5) and (A6), we obtain the expression for the power loss in the dielectric medium as

$$\frac{P_l^d}{\Delta y} = \frac{k_0 H^2\tan\delta}{\epsilon_0\omega\epsilon^2 a^2}[\gamma(2-\epsilon\beta^2) + \epsilon^2\beta^2 k_0 d(1+a^2)]. \quad \text{(A9)}$$

Now, Eqs. (A7) and (A9) are used in Eq. (A8) to obtain the dielectric attenuation coefficient as

$$\alpha^d = \frac{k_0\tan\delta}{2}\frac{[\gamma(2-\epsilon\beta^2) + \epsilon^2\beta^2 k_0 d(1+a^2)]}{[\gamma(1+\epsilon^2 a^2) + \epsilon k_0 d(1+a^2)]}. \quad \text{(A10)}$$

In region III, which consists of metal, the dissipation of power occurs as Ohmic losses due to finite conductivity of the metal. Here, we have assumed that the dissipation occurs in a very small region near the metallic surface. The power loss per unit length along the metallic surface is given by $P_l^c = (R_s/2)\int|H_y|^2 dy$ [64], where the integration is carried out over length Δy in the y-direction. The magnitude of electromagnetic field H_y at the metallic surface as given in Eq. (A4) is used to evaluate P_l^c. By performing the required algebra for P_l^c, and using it along with Eq. (A7) for P_t in Eq. (A8), the following expression for Ohmic attenuation coefficient is obtained:

$$\alpha^c = \frac{R_s}{Z_0}\frac{\beta\epsilon^2 k_0(1+a^2)}{[\gamma(1+\epsilon^2 a^2) + \epsilon k_0 d(1+a^2)]}. \quad \text{(A11)}$$

The sum of dielectric losses and losses due to finite conductivity of the metal gives total losses present in the system and we write the total attenuation coefficient α of the surface mode as $\alpha = \alpha^d + \alpha^c$.

[1] M. Danos, S. Geschwind, H. Lashinsky, and A. V. Trier, Čerenkov effect at microwave frequencies, Phys. Rev. **92**, 828 (1953).

[2] M. Danos, Čerenkov radiation from extended electron beams, J. Appl. Phys. **26**, 2 (1955).

[3] J. Walsh, B. Johnson, G. Dattoli, and A. Renieri, Undulator and Cerenkov Free-Electron Lasers: A Preliminary Comparison, Phys. Rev. Lett. **53**, 779 (1984).

[4] J. E. Walsh, B. Johnson, C. Shaughnessy, F. Ciocci, G. Dattoli, A. Angelis, A. Dipace, E. Fiorentino, G. P. Gallerano, T. Letardi *et al.*, A 100 μm Cherenkov laser experiment, Nucl. Instrum. Methods Phys. Res., Sect. A **250**, 308 (1986).

[5] F. Ciocci, G. Dattoli, A. Angelis, A. Dipace, A. Doria, E. Fiorentino, G. P. Gallerano, T. Letardi, A. Marino, A. Renieri *et al.*, Status of the ENEA-Dartmouth far infrared Cherenkov laser experiment, Nucl. Instrum. Methods Phys. Res., Sect. A **259**, 128 (1987).

[6] E. P. Garate, J. Walsh, C. Shaughnessy, B. Johnson, and S. Moustaizis, Cherenkov free electron laser operation from 375 to 1000 μm, Nucl. Instrum. Methods Phys. Res., Sect. A **259**, 125 (1987).

[7] J. Walsh, C. Shaughnessy, R. Layman, G. Dattoli, G.-P. Gallerano, and A. Renieri, Preliminary results from a microwave-driven 100 μm wavelength Cherenkov FEL

experiment, Nucl. Instrum. Methods Phys. Res., Sect. A **272**, 132 (1988).

[8] F. Ciocci, A. Doria, G. P. Gallerano, I. Giabbai, M. F. Kimmitt, G. Messina, A. Renieri, and J. E. Walsh, Observation of Coherent Millimeter and Submillimeter emission from a Microtron-Driven Cherenkov Free-Electron Laser, Phys. Rev. Lett. **66**, 699 (1991).

[9] E. E. Fisch and J. E. Walsh, Opertation of the sapphire Cerenkov laser, Appl. Phys. Lett. **60**, 1298 (1992).

[10] Y. Seo, E. H. Choi, and G. S. Cho, Radiation growth characteristics of a two-dimensional micro-Cherenkov free-electron laser, J. Phys. D **33**, 654 (2000).

[11] I. J. Owens and J. H. Brownell, High-order Čerenkov laser gain, Phys. Rev. E **67**, 036611 (2003).

[12] I. J. Owens and J. H. Brownell, Compact superradiant Čerenkov source, J. Appl. Phys. **97**, 104915 (2005).

[13] M. R. Asakawa, K. Nakao, M. Kusaba, and Y. Tsunawaki, Developement of a compact Cherenkov free-electron laser in terahertz spectral range, in *Proceedings of the FEL Conference* (JACoW, Berlin, 2006), pp. 364–367.

[14] N. Miyabe, A. Ikeda, M. R. Asakawa, M. Kusaba, and Y. Tsunawaki, Developement of a compact Cherenkov free-electron laser operating in terahertz wave range, in *Proceedings of the 29th Free Electron Laser Conference, Novosibirsk, Russia* (BINP, Novosibirsk, 2007), pp. 406–408.

[15] H. L. Andrews and C. A. Brau, Three-dimensional theory of the Cerenkov free-electron laser, J. Appl. Phys. **101**, 104904 (2007).

[16] D. Li, G. Huo, K. Imasaki, M. Asakawa, and Y. Tsunawaki, Nonlinear analysis of Cherenkov free-electron laser with double-slab structure, Infrared Phys. Technol. **53**, 204 (2010).

[17] D. Li, Y. Wang, M. Hangyo, Y. Wei, Z. Yang, and S. Miyamoto, Cherenkov radiation oscillator without reflectors, Appl. Phys. Lett. **104**, 194102 (2014).

[18] Y. Kalkal and V. Kumar, Analysis of Čerenkov free-electron lasers, Phys. Rev. ST Accel. Beams **18**, 030707 (2015).

[19] L. Schachter and A. Ron, Smith-Purcell free-electron laser, Phys. Rev. A **40**, 876 (1989).

[20] B. Hafizi, P. Sprangle, and P. Serafim, Nonlinear analysis of a grating free-electron laser, Phys. Rev. A **45**, 8846 (1992).

[21] J. Urata, M. Goldstein, M. F. Kimmitt, A. Naumov, C. Platt, and J. E. Walsh, Superradiant Smith-Purcell Emission, Phys. Rev. Lett. **80**, 516 (1998).

[22] K.-J. Kim and S.-B. Song, Self-amplified spontaneous emission in Smith-Purcell free-electron lasers, Nucl. Instrum. Methods Phys. Res., Sect. A **475**, 158 (2001).

[23] H. L. Andrews and C. A. Brau, Gain of a Smith-Purcell free-electron laser, Phys. Rev. ST Accel. Beams **7**, 070701 (2004).

[24] H. L. Andrews, C. H. Boulware, C. A. Brau, and J. D. Jarvis, Dispersion and attenuation in a Smith-Purcell free electron laser, Phys. Rev. ST Accel. Beams **8**, 050703 (2005).

[25] V. Kumar and K.-J. Kim, Analysis of Smith-Purcell free-electron lasers, Phys. Rev. E **73**, 026501 (2006).

[26] K.-J. Kim and V. Kumar, Electron beam requirements for a three-dimensional Smith-Purcell backward-wave oscillator for intense terahertz radiation, Phys. Rev. ST Accel. Beams **10**, 080702 (2007).

[27] V. Kumar and K.-J. Kim, Electron beam requirements for Smith-Purcell backward wave oscillator with external focusing, Phys. Rev. ST Accel. Beams **12**, 070703 (2009).

[28] V. Kumar and K.-J. Kim, Three-dimensional analysis of the surface mode supported by a reflection grating, in *Proceedings of the 29th Free Electron Laser Conference, Novosibirsk, Russia* (Ref. [14]), pp. 38–41.

[29] J. Gardelle, L. Courtois, P. Modin, and J. T. Donohue, Observation of coherent Smith-Purcell radiation using an initially continuous flat beam, Phys. Rev. ST Accel. Beams **12**, 110701 (2009).

[30] H. L. Andrews, C. A. Brau, J. D. Jarvis, C. F. Guertin, A. O'Donnell, B. Durant, T. H. Lowell, and M. R. Mross, Observation of THz evanescent waves in a Smith-Purcell free-electron laser, Phys. Rev. ST Accel. Beams **12**, 080703 (2009).

[31] J. T. Donohue and J. Gardelle, Dispersion relation for a three-dimensional lamellar grating, Phys. Rev. ST Accel. Beams **14**, 060709 (2011).

[32] D. Clery, Brainstorming their way to an imaging revolution, Science **297**, 761 (2002).

[33] P. H. Siegel, Terahertz technology, IEEE Trans. Microwave Theory Tech. **50**, 910 (2002).

[34] A. E. Siegman, *Lasers* (University Science Books, Mill Valley, California, 1986).

[35] K.-J. Kim, Characteristics of synchrotron radiation, in *AIP Conference Proceedings No. 184* (AIP, Fermilab/Cornell University, New York, 1989), pp. 565–632.

[36] F. Pampaloni and J. Enderlein, Gaussian, Hermite-Gaussian, and Laguerre-Gaussian beams: A primer, arXiv: physics/0410021.

[37] T. P. Horikis and M. S. McCallum, Self-Fourier functions and self-Fourier operators, J. Opt. Soc. Am. A **23**, 829 (2006).

[38] V. Kumar and K.-J. Kim, Optimization of parameters of Smith-Purcell BWO, in *Proceedings of the FEL Conference* (Ref. [13]), pp. 67–70.

[39] V. Kumar and K.-J. Kim, Calculation of reflection matrix elements of a grating for growing evanescent waves, in *Proceedings of the 21st Particle Accelerator Conference, Knoxville, TN* (IEEE, Piscataway, NJ, 2005), pp. 1616–1618.

[40] C. A. Brau, *Free-Electron Lasers* (Academic Press, San Diego, 1990).

[41] A. Chao, *Physics of Collective Beam Instabilities in High Energy Accelerators* (John Wiley & Sons, Inc., New York, 1993).

[42] P. Piot, Y.-E. Sun, and K.-J. Kim, Photoinjector generation of a flat electron beam with transverse emittance ratio of 100, Phys. Rev. ST Accel. Beams **9**, 031001 (2006).

[43] E. Scharlemann, Wiggle plane focusing in linear wigglers, J. Appl. Phys. **58**, 2154 (1985).

[44] J. H. Booske, W. W. Destler, Z. Segalov, D. J. Radack, E. T. Rosenbury, J. Rodgers, T. M. Antonsen, V. L. Granatstein, and I. D. Mayergoyz, Propagation of wiggler focused relativistic sheet electron beams, J. Appl. Phys. **64**, 6 (1988).

[45] D. Li, Z. Yang, K. Imasaki, and G.-S. Park, Particle-in-cell simulation of coherent and superradiant Smith-Purcell radiation, Phys. Rev. ST Accel. Beams **9**, 040701 (2006).
[46] J. T. Donohue and J. Gardelle, Simulation of Smith-Purcell terahertz radiation using a particle-in-cell code, Phys. Rev. ST Accel. Beams **9**, 060701 (2006).
[47] R. Brinkmann, Y. Derbenev, and K. Flöttmann, A low emittance, flat-beam electron source for linear colliders, Phys. Rev. ST Accel. Beams **4**, 053501 (2001).
[48] J. H. Booske, B. D. McVeya, and T. M. Antonsen, Stability and confinement of nonrelativistic sheet electron beams with periodic cusped magnetic focusing, J. Appl. Phys. **73**, 4140 (1993).
[49] K. T. Nguyen, J. A. Pasour, T. M. Antonsen, P. B. Larsen, J. J. Petillo, and B. Levush, Intense sheet electron beam transport in a uniform solenoidal magnetic field, IEEE Trans. Electron Devices **56**, 744 (2009).
[50] W. Westphal and A. Sils, Massachusetts Institute of Technology, Technical Report No. AFML-TR-72-39, 1972.
[51] D. B. Tanner and D. C. Larson, Electrical resistivity of silver films, Phys. Rev. **166**, 652 (1968).
[52] J. Zhu, P. Piot, D. Mihalcea, and C. R. Prokop, Formation of compressed flat electron beams with high transverse-emittance ratios, Phys. Rev. ST Accel. Beams **17**, 084401 (2014).
[53] R. Forman and D. H. Smith, Thermionic cathode life-test studies, IEEE Trans. Electron Devices **26**, 1567 (1979).
[54] A. Taran, D. Voronovich, S. Plankovskyy, V. Paderno, and V. Filipov, Review of LaB_6, Re-W dispenser, and $BaHfO_3$-W cathode development, IEEE Trans. Electron Devices **56**, 812 (2009).
[55] J. A. Clarke, *The Science and Technology of Undulators and Wigglers* (Oxford University Press, New York, 2004).
[56] B. Peterson, O. Oniku, W. Patterson, D. L. Roy, A. Garraud, F. Herrault, N. Dempsey, D. Arnold, and M. Allen, Technology development for short-period magnetic undulators, Phys. Procedia **52**, 36 (2014).
[57] B. E. Carlsten, L. M. Earley, F. L. Krawczyk, S. J. Russell, J. M. Potter, P. Ferguson, and S. Humphries, Stability of an emittance-dominated sheet-electron beam in planar wiggler and periodic permanent magnet structures with natural focusing, Phys. Rev. ST Accel. Beams **8**, 062001 (2005).
[58] L. Reimer and H. Kohl, *Transmission Electron Microscopy*, Springer Series in Optical Sciences (Springer-Verlag, Berlin, 1999), Vol. 36.
[59] K. Togawa, T. Shintake, H. Baba, T. Inagaki, K. Onoe, T. Tanaka, and H. Matsumoto, Low emittance 500 kV thermionic electron gun, in *Proceedings of the LINAC Conference* (JACoW, Lübeck, 2004), pp. 261–265.
[60] G. Dattoli, A. Renieri, and A. Torre, *Lectures on the Free Electron Laser Theory and Related Topics* (World Scientific, Singapore, 1993).
[61] S. Reiche, GENESIS 1.3: A fully 3D time-dependent FEL simulation code, Nucl. Instrum. Methods Phys. Res., Sect. A **429**, 243 (1999).
[62] S. Y. Liao, *Microwave Devices and Circuits* (Dorling Kindersley, India, 2011).
[63] R. A. Waldron, *Theory of Guided Electromagnetic Waves* (Van Nostrand Reinhold, New York, 1970).
[64] J. D. Jackson, *Classical Electrodynamics* (John Wiley, Singapore, 1999).